Twenty-Fifth Symposium (International) on Combustion/The Combustion Institute, 1994/pp. 1685–1692

BUOYANT DOWNWARD DIFFUSION FLAME SPREAD AND EXTINCTION IN PARTIAL-GRAVITY ACCELERATIONS

KURT R. SACKSTEDER
NASA Lewis Research Center
21000 Brookpark Road, Cleveland, OH 44135, USA

AND

JAMES S. T'IEN
Case Western Reserve University
Cleveland, OH 44106, USA

This paper describes experimental observations of downward, opposed-flow flame spreading made under partial-gravity conditions aboard NASA research aircraft. Special apparatus and techniques for these tests are described, including schlieren imaging of dim near-limit flames. Flame-spreading and flammability limit behaviors of a thin cellulosic fuel, 1×10^{-3} g/cm^2 tested at 1 atm of pressure in oxygen/nitrogen mixtures of 13–21% oxygen by volume, are described for effective acceleration levels ranging from 0.05 to 0.6 times normal earth gravity (1 g). Downward-burning flammability increases in partial gravity, with the limiting oxygen fraction falling from 15.6% oxygen in 1 g to 13–14% oxygen in 0.05–0.1 g. Flame-spread rates are shown to peak in partial gravity, increasing by 20% over the 1-g value in air (21% oxygen). Partial-gravity flame-spreading results, corrected for fuel density and thickness, are consistent with results obtained at acceleration levels above 1 g in a centrifuge. The results compare qualitatively with predictions of flame spreading in buoyant flow by models that include finite-rate chemical kinetics and surface and gas-phase radiative loss mechanisms. A correlation of experimental buoyant downward flame-spread results is introduced that accounts for radiative heat losses using a dimensionless spread rate, V_f^*, a radiation/conduction number, S_n, and the Damkohler number, Da, as parameters. The correlation includes data from 0.05 g to 4.25 g and oxygen/nitrogen mixtures from 14% to 50% oxygen.

Introduction

Flame spreading over solid fuels is a phenomena of fundamental interest and of practical value in the study and control of fire. In flame-spread studies, distinctions between flames in flows opposed to and concurrent with the flame-spread direction, between thermally thin and thick fuels, and between flows imposed externally (forced) or by gravity (buoyancy) have been identified. Several reviews articulate the subject [1,2].

Access to microgravity environments motivated theoretical and experimental explorations of low-speed flow regimes in which buoyancy forces could be reduced or eliminated. Numerical modeling quantified surface and gas-phase radiation mechanisms [3–6] and predicted the influence of radiative loss in spread-rate reductions and quenching. Numerical evaluations of velocity-profile effects [7] and predictions that near-wall velocity gradients would correlate spreading behavior [8] led us to suggest separate experimental observations of flames spreading in low-speed purely forced and purely buoyant flows.

Purely forced, opposed-flow, and quiescent studies in microgravity, using drop-tower [9,10] and space shuttle facilities [11], demonstrated the predicted spread rate and quenching effects. In purely buoyant flow, however, downward-burning experiments were limited to normal earth gravity (1 g) and elevated gravity using a centrifuge [12]. While noting a low-gravity, quiescent study perturbed by unsteady accelerations [13], this paper reports the first systematic observations of flames spreading in purely buoyant, low-speed flows induced by accelerations below 1 g.

We conducted a series of aircraft-based tests to observe both downward and upward flame-spreading and flammability behavior of thin solid fuels in sustained partial-gravity accelerations between 0.05 and 1 g. To obtain these data, special apparatus and techniques were developed. This paper concerns the downward-spreading case only and provides an opportunity to evaluate models of flame spreading in purely buoyant flow.

Experiments

An apparatus was devised to observe flame spread over solid fuels in partial-gravity accelerations aboard

NASA aircraft facilities. The apparatus provides semiautonomous operation, capable of several tests per flight, either attached to the airframe or floated freely in the aircraft cabin. The apparatus includes a 26-liter cylindrical chamber, 25.4 cm in diameter and 50.8 cm in length; simultaneous schlieren and conventional imaging; provisions for atmosphere replacement; thermocouple, ignition, and lighting circuitry; and a flanged end plate with a quick-release binding for rapid specimen replacement.

Test specimens, 8-cm long and 7-cm wide, were made of thin cellulosic tissues (tradename Kimwipes), which were used previously in drop-tower tests [9,10,14]. This material has a half-thickness area density (i.e., mass density × thickness) of 1.0 mg/cm^2 and was used because of its high flame-spread rate compared to other fuels and because it tends to remain flat while burning. The samples were taped across a 25.4 × 5 cm gap in 0.05-cm-thick stainless-steel sample holders that fill a diametrical plane of the cylindrical chamber, thereby exposing fuel, 8 cm in the (axial) burning direction by 5-cm wide, to the atmosphere on both sides.

Control of the fuel moisture content was constrained. Prior to takeoff, premounted samples were stored in vacuum for approximately 1 hour. At altitude, where atmospheric moisture content is low, the samples were exposed to the aircraft cabin. A vacuum exposure in the test chamber before filling and ignition lasted approximately 1 min. Samples were ignited by resistance-heating a thin wire for 0.10 s, releasing 36 j to ignite a strip of nitrocellulose (10.5 mg, +/−1%), releasing an additional 26 j [15] in a flame ball, bathing the ignition region. This technique provided a consistent deposition of ignition energy compared to the hot wire used alone.

The test atmosphere was replaced for each test. After replacing the spent test specimen, the chamber was evacuated to a pressure of less than 0.008 atm and then filled with a commercial oxygen/nitrogen mixture certified to +/−0.03% absolute oxygen content. The residual air after evacuation introduced <0.06% error absolute oxygen content. All experiments were conducted at an initial pressure of 1 atm, measured with a transducer calibrated daily.

Flames were visualized with a color schlieren system [16]. The schlieren system was sensitive to the component of the refractive-index gradient normal to the fuel surface, in a cylindrical detection volume 7.9 cm in diameter. Ray deflections, attributed to flame-induced density variations, were discriminated at the image plane of the schlieren mirror using a color transparency varying linearly in hue with lateral displacement and then imaged with a video camera. Conventional images of the top view of the flames were recorded using a 16-mm motion picture camera operating at 24 frames/s.

The tests were conducted aboard the NASA KC-135 at the NASA Johnson Space Center flying Keplerian trajectories (parabolas) to simulate gravitational accelerations between 0.05 and 0.6 g, including lunar (0.16 g) and martian (0.38 g) levels [17]. The first parabolas ever attempted at 0.05 and 0.6 g were performed for these tests. Local three-axis accelerations were measured with a duplicate of the NASA Space Accelerometer Measurement System [18].

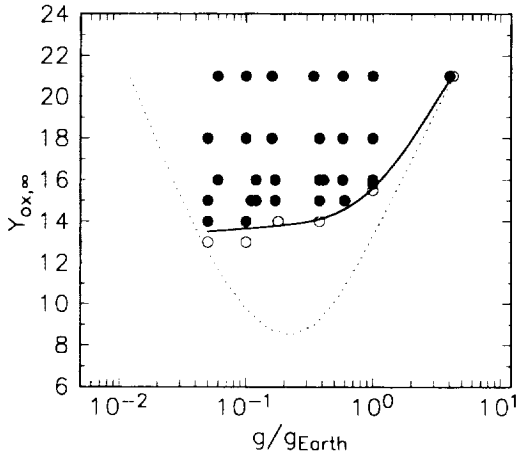

FIG. 1. Flammability map in O_2 mole fraction vs acceleration for thin cellulosic fuels, with downward burning in purely buoyant flows in 1-atm pressure. Solid symbols represent flammable conditions; hollow symbols represent nonflammable conditions. Data near 4 g are from Ref. 12. The solid line estimates experimental flammability boundary; the dotted line is the boundary predicted in Ref. 6. The microgravity limit, not shown, is reported as 21% O_2 [9].

Results

Acceleration Environment:

Wind, atmospheric turbulence, and pilot and aircraft performance introduced continuous variation into the measured acceleration levels. Parabolas at the lowest set points (0.05–0.10 g) were perturbed typically by high-frequency (>1 Hz) variations, often called g-jitter, of about 0.02 g. Higher set points (0.16–0.6 g) were additionally perturbed by lower-frequency variations (≈0.2–1.0 Hz) of about 0.04 g. The average duration of the parabolas increased with partial-gravity level, from about 8 s for the shortest 0.05-g parabola to about 50 s for most 0.6-g parabolas. The parabolas begin and end with a pull-up maneuver at just under 2.0 g acceleration, to which some flames were exposed.

Flammability:

Figure 1 summarizes the test matrix and shows a flammability boundary based on acceleration level

and atmospheric oxygen content. In 1 g, the same apparatus and fuel (5-cm wide) were used to determine the limit using partial-pressure mixtures of the certified 15% and 16% mixtures. In 1 g, the specimens never burned more than 2–3 cm below the ignitor in 15.5% O_2; they usually burned 4–5 cm, but never the full 8 cm, in 15.6% O_2; and they usually, but not always, burned the full 8 cm in 15.7% O_2. Completely burning 0.08 gm of cellulose reduces (by calculation) the oxygen in the chamber from 15.6 to 15.53%, constraining the limit determination to a precision of about 0.1%. Based on the behavior described, a 1-g limit of 15.6% O_2 is shown in Fig. 1.

Obtaining the precision of the 1-g limit criteria was not practical in the aircraft because test opportunities were limited. In 14% O_2 at 0.18 g and 0.38 g, flames propagated 1.4 and 0.4 cm, respectively, and quenched before the onset of high accelerations, while in 15% O_2 (same accelerations), the samples burned completely. In 14% O_2 at 0.05 g and 0.1 g, flames progressed 3.1 and 2.4 cm, respectively, spreading in partial gravity for 8–9 s and then extinguishing during high accelerations. These are interpreted as flammable conditions. Samples ignited in 13% O_2 quickly quenched.

The reported 1-g downward-burning limit of 16.0–16.5% O_2 for 3-cm-wide samples of this fuel [9] was higher than results obtained with 3-cm-wide samples in the aircraft apparatus, where using the above propagation criteria provided a limit of 15.8% O_2. The earlier tests were ignited with a heated wire and may have been influenced by a nearby mirror present to obtain an orthogonal view. The higher flammability limit might be attributed to differences in the useful ignition energy or heat losses to the mirror. This comparison suggests that the quiescent microgravity limit of 21% O_2 (the logical extreme of the buoyant-flow case), obtained in drop-tower tests [9], is reasonable to within 1% O_2. However, because drop-tower accelerations have not been measured, that limit could not be included in Fig. 1. Limiting accelerations between 4.0 and 4.25 g in 21% O_2 for a similar fuel were reported in centrifuge tests [12] and are shown in Fig. 1.

Reducing accelerations from 4 to 0.05 g monotonically enhances downward-burning flammability. The microgravity limit of 21% O_2 implies, however, that the flammability boundary curves upward at smaller accelerations and that a minimally flammable oxygen environment exists for this fuel, for downward burning, at or below 0.05 g. The analogous flammability boundary, predicted by a numerical model [6], is included in Fig. 1 for comparison and later discussion.

Flame Imaging:

Recorded schlieren flame images were fundamentally different from earlier gravity-related flame-spreading results. Visible-light emissions from near-limit flames in microgravity tests are dim and difficult to capture by direct imaging, either by video or by motion picture film [9–11,13,14]. Measures to enhance film images, including forced film processing, low framing rates, and small *f*/numbers, reduce flame-tracking precision. Short focal-length lenses, typical of compact microgravity experiment designs, introduce spatial distortions from magnification variations across wide flames.

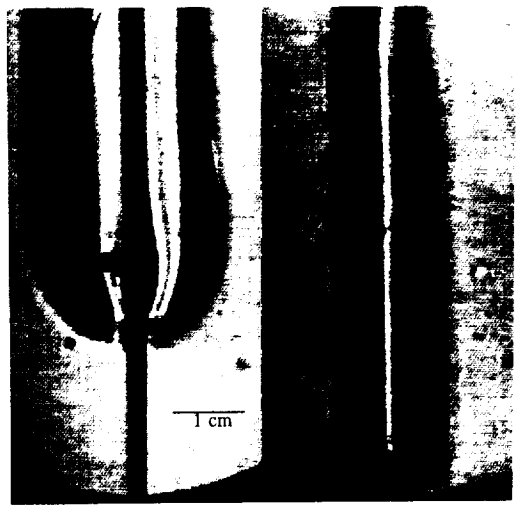

FIG. 2. Rainbow schlieren images of downward-burning thin fuel in 15% O_2: on the left at 0.10 g/g_{earth} on the right near the blowoff limit at 0.6 g/g_{earth}.

Schlieren imaging provided increased dim-flame detection sensitivity and constant image magnification across the flame width. At ignition, an expanding ball of heated gases was visible to the schlieren system, reaching 2–3 cm below (upstream of) the ignitor (for <1 s) before buoyancy displaced it upward. Conventional visible photography showed a smaller flame surrounding the ignitor. Extinguishing flames were clearly defined in the schlieren images, shrinking to $\leq$2–3 mm in length before disappearing. Figure 2 shows schlieren images of a flame spreading first at 0.1 g in 15% O_2, a nonflammable condition in 1 g, and then, as the flame nears blowoff extinction, at higher accelerations at the end of the test.

Flame Spread:

Flame propagation rates were obtained from the schlieren results. Figure 3 shows the flame displacement with time, synchronized with the component parallel to the flame spreading direction of the instantaneous local acceleration, for a test in 15% O_2, where the slope of the displacement plot indicates flame-spread rate. At the end of the parabola, the increase in local acceleration accompanied a slowed,

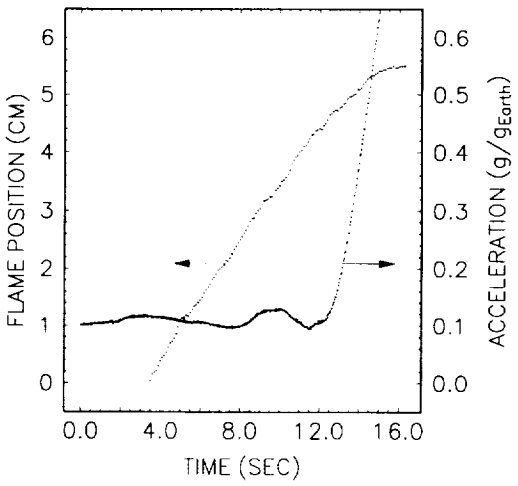

FIG. 3. Synchronized-spreading flame position and local acceleration vs time for downward-burning thin fuel in 15% O_2.

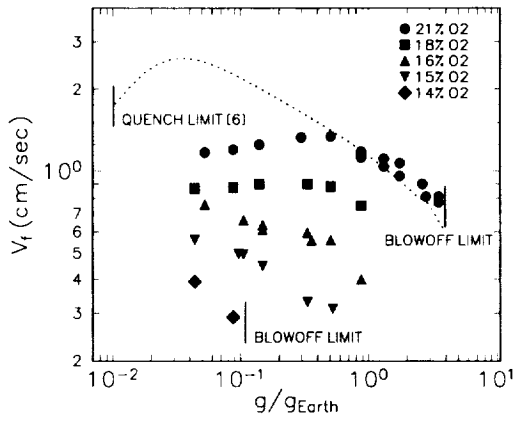

FIG. 4. Flame-spread rates of thin cellulosic fuels in O_2/N_2 mixtures at 1-atm pressure vs local acceleration. Data above 1 g/g_{earth} are from Ref. 12. The dotted line represents predicted spread rates from Ref. 6. Vertical lines represent flammability limits: blowoff limits at higher accelerations (14% from this work, 21% from Ref. 12) and radiative quenching limit at lower acceleration (theoretical prediction [6]).

then extinguished, flame. Figure 2 shows schlieren images from that test before and during the higher accelerations, illustrating how the flame narrowed as it approached extinction. The flame was extinguished as the local accelerations crossed the flammability boundary of Fig. 1, at about 0.6 g.

Spread rates were influenced by g-jitter to the extent that reporting spread rates averaged over the test time showed unacceptable scatter. The partial-gravity results, shown in Fig. 4, were obtained, instead, by measuring flame displacements during brief time periods, ≥3 s, of smaller g-jitter. This procedure was considered acceptable since flames responded to perturbations in much less than 1 s (e.g., at time 10 s in Fig. 3). Figure 4 also includes 1-g results, obtained in the aircraft, drop-tower [9], and centrifuge [12] test chambers, and centrifuge data in 21% O_2 up to 4.25 g. All spread rates are corrected for fuel area density, ρ_{area}, where $\rho_{area} = \rho_{mass} \cdot \tau$, the mass density times the fuel half-thickness. This correction follows from the assertion in the early heat transfer model [19] that $\rho_{area} \cdot V_f$ = constant for thin fuels and has been used successfully [9,10,12].

Partial-gravity spread rates in 21% O_2 fall naturally along the trend of the centrifuge data, peak at an acceleration level near 0.6 g, then decline with further decreases in acceleration. Spread rates at 1 g from the three different test chambers agree to within 5%. Prediction of spread-rate behavior for a thin fuel in 21% O_2 from a numerical model [6], corrected for ρ_{area} is included for comparison and later discussion. Spread rates in 18% O_2 show a similar nonmonotonic spread-rate variation with acceleration. Spread rates in 14–16% O_2 show only the downward slope.

Discussion

Comparison with Theory:

Two numerical models predict downward flame-spreading behavior at partial-gravity accelerations [6,8]. Both calculations utilize a one-step, finite-rate, gas-phase chemical reaction model and estimate radiative losses from both the fuel surface and the gas phase. Reference 8 presents calculated spread rates and extinction limits in 50% O_2–50% N_2, at 1.5 atm, from 10^{-6} g to 10 g, and in 21% O_2–79% N_2 at 1–4 g. Reference 6 presents spread rates and extinction limits in 21% O_2–79% N_2, at 1 atm from 0.012 to4.3 g, and a flammability boundary over the same range of accelerations. The data of Ref. 6 are included as the dotted lines in Figs. 1 and 4.

The predictions of spread rate show qualitatively the peak spread-rate feature observed experimentally in 21% and 18% O_2 at intermediate gravity levels. From the peak, falling spread rates at higher gravity are attributed to decreased reactant residence time in the flame zone (compared to the chemical reaction time) and reduced forward heat transfer from flames receding with respect to the pyrolysis front. Falling spread rates at lower gravity are attributed to lower flame temperatures, resulting from an increasing ratio of radiative loss to chemical heat release, and reduced forward heat transfer from cooler flames
farther from the fuel surface. The spread-rate predictions of Ref. 6 for 21% O_2 are higher (Fig. 4) than experimentally observed in partial gravity, though

they agree well with experiments at normal gravity and above. The predictions in Ref. 8 also reproduce the observed experimental results at and above 1 g in 21% O_2, as shown , and also in 50% O_2, at 1.5 atm.

Both models predict a high-gravity extinction limit (*viz.* , a blowoff limit) and a low-gravity extinction limit (*viz.* , a radiative quenching limit). These flammability limits are attributed to the dominance of the flame-retarding mechanisms described above. The flammability boundary predicted in Ref. 6 (Fig. 1) is U-shaped, showing a minimally flammable oxygen concentration between 0.2 *g* and 0.3 *g*. The flammability boundary suggested by the experimental data does not show such a minimum, but the reported quiescent microgravity limit for this fuel, 21% O_2 [9], suggests that it exists $\leq$0.05 g. The predicted flammability boundary agrees well with experimental observations above normal gravity but diverges from the observed boundary at normal gravity (13.2 vs 15.6% O_2) and below (21% O_2 limit at 0.012 *g* vs $\approx$microgravity [9]).

The sources of discrepancy between prediction [6] and observed partial-gravity flammability and spread-rate behavior are not clear but may involve the choice of kinetic and radiation parameters. The spread-rate peak and the (presumed) minimum-oxygen limit arise from competition, under finite kinetics, between the heat-release rate reduction (due to shortened residence time) and the radiative heat-loss rate. An underestimation of the radiative loss rate compared to the chemical reaction rate might explain the differences at 1 g and the partial-gravity levels but would not reconcile the limiting accelerations in 21% oxygen.

Flame Spread-Rate Correlation:

Correlations of measured flame-spread rates have been achieved for purely buoyant flows [12] and for forced-convection flows in normal gravity [20] using formulations of dimensionless spread rate, V_f°, vs Damkohler number, *Da*. Formulations of *Da*, nominally a ratio of reactant residence time in the flame to chemical reaction time, have included simple pre-exponential chemical models (without Arrhenius factors) [21,6], models with strong flame temperature dependence [12], and additional provisions for fuel-vapor diffusion from the surface [20]. Velocity characterizations for residence-time estimates have included a buoyant velocity, $V_b \approx (\alpha g(T_f - T_\infty)/T_\infty)^{1/3}$ [21,12,8], where T_f and T_∞ are flame and ambient temperatures, and α is the thermal diffusivity, or the free stream velocity, U_∞, alone [20] or including consideration of the boundary-layer structure [22]. The term V_f°, corrected for ρ_{area}, is a ratio of actual spread rate to the spread rate possible without heat loss in the infinite chemical-rate limit [19]. Where the flame-retarding mechanism is associated with limited residence time, *Da* correlations of flame-spread rates are successful. This approach neither succeeds with data from microgravity-forced flows nor with partial-gravity data, because it does not account for radiative losses from these flames.

We revisited the formulation of the data correlation for purely buoyant flame-spread data [12], to include the partial-gravity data. We evaluated *Da* similarly:

$$Da = \frac{B\lambda m_{OX,\infty}}{c_p M_{OX} V_b^2} \cdot \left[\frac{RT_f}{E} \cdot \frac{T_f}{\left(\frac{\Delta H_c m_{OX,\infty}}{i c_p} \right)} \right]^3 \cdot \exp\left(- \frac{E}{RT_f} \right)$$

where the pre-exponential constant $B = 5.69 \cdot 10^9$ m^3/mole-s; the activation energy $E = 167.35$ Kj/Kg-K; the heat of combustion $\Delta H_c = 16{,}740$ Kj/Kg; $m_{OX,\infty}$ and M_{OX} are the ambient O_2 mass fraction and molecular weight, respectively; the stoichiometric oxygen/fuel mass ratio $i = 1.185$; and λ and c_p are the gas thermal conductivity and specific heat, evaluated for the initial O_2/N_2 mixtures at the fuel vaporization temperature $T_v = 618$ K. We evaluated T_f differently, however, using the STANJAN equilibrium code for a stoichiometric, adiabatic flame temperature, allowing for dissociation, and we evaluated V_b using T_f. The pre-exponential constant, which does not affect the shape of the resulting data presentation, was adjusted from the literature value [12] to bring $Da = 1$ at blowoff extinction. The grouping $(\Delta H_c m_{OX,\infty}/ic_p)$ in the cubic factor is a reference temperature [12] that varies only with the explicit O_2 content.

The dimensionless spread rate, defined [12] as

$$V_f^\circ = \frac{V_f}{V_{f,\infty}} = \rho_{area} V_f \cdot \frac{c_s(T_v - T_s)}{\sqrt{2}\lambda(T_f - T_s)}$$

where $V_{f,\infty}$ is the spread rate in the no-loss, infinite-kinetics limit, and the solid-fuel specific heat $c_s = 1.26$ Kj/Kg-K. A radiation parameter, S_R, derived through a dimensional analysis of the energy equation [3,4,6] as a ratio of radiation to conduction over one thermal length, $S_R = (\sigma T_r^4)/[\lambda T_r/(\alpha/V_r)] = \sigma T_r^3/\rho c_p V_r$, where σ is the Stefan–Boltzmann constant and V_r is the reference velocity for the flow (in the buoyant case, $V_r = V_b$). We have used S_R as a correction to V_f°, suggesting that it estimates the additional spread-rate deficit, due to radiative heat loss, from the no-loss maximum spread rate. Figure 5 shows a plot of $V_f^\circ \cdot S_R$ vs *Da* for flames spreading in purely buoyant flow, in partial gravity (data of Fig. 4), and in the centrifuge (21% O_2 and 50% O_2 1 atm from 1 g to 4 g [12]).

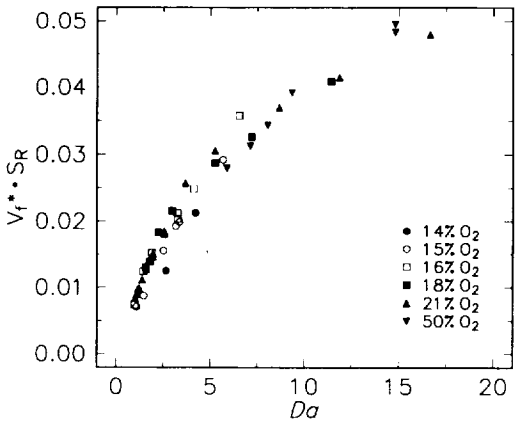

FIG. 5. Dimensionless spread rate corrected using a radiation parameter, $S_R = \sigma T_\infty / \rho c_p V_\infty$ vs Damkohler number for downward burning of thin cellulosic fuels; 50% O_2 data obtained in $g/g_{earth} > 1$ [12], 21% O_2 obtained from $g/g_{earth} = 0.05$–4.25 (>1 g from Ref. 12). Pre-exponential constant in Da adjusted so that $Da = 1$ at blowoff extinction.

We considered that calculating T_f independently, while using c_p and ΔH_c evaluated as in Ref. 12, might suggest an inconsistency in evaluating $V_f^* \cdot S_R$ and Da. The T_f values estimated using ΔH_c, c_p evaluated at T_∞ for the O_2/N_2 mixture, without dissociation [12], are much higher than ours, which we believe to be more realistic. A correct c_p value is implicit, however, in the equilibrium calculation, allowing dissociation, of T_f. Remaining uncertainty in calculating T_f lies in the chosen value of ΔH_c, which both formulations use. The roles of c_p and λ in $V_f^* \cdot S_R$ and Da are primarily associated with forward heat conduction, so the evaluation for the ambient O_2/N_2 mixture at an intermediate temperature, T_∞, is appropriate. The constants ΔH_c, i, and c_p in the reference temperature do not affect the shape of the data presentation.

This presentation smooths the scatter in spread rates seen in Fig. 4. The scatter has no trend attributable to O_2 content. The data in 21% O_2 span the acceleration range of 0.05–4.25 g and also the length of the correlation curve, while the data in 50% O_2 span only 1–4 g and lie within the 21% O_2 data. Near blowoff extinction, $V_f^* \cdot S_R$ vs Da values for 15% O_2 at 0.6 g, 15.6% O_2 at 1 g, and 21% O_2 at 4.25 g lie together at the left-hand end of the curve.

The question arises whether the low-gravity extinction boundary predicted [6] would, like the blowoff extinction, have similar Da for varying g and oxygen contents. Since the predicted low-gravity quenching was not observed in the attainable acceleration range, we cannot determine any quenching values for Da or the nature of the $V_f^* \cdot S_R$ curve at the quenching point. Using an adiabatic T_f, Da increases with oxygen content (i.e., the chemical rate increases faster than V_f) and with decreasing acceleration. Since the flammability boundary prediction [6] suggests that quenching in decreasing accelerations would be observed first in lower O_2 environments, we suggest that a correlation of quenching limits cannot be achieved until the T_f estimate used in Da is altered to represent the cooling effect of radiative loss.

As numerical predictions suggest [8], we attempted to include forced-flow flame-spread data [9,10,20] into this correlation, using the free-stream velocity $V_\infty = U_\infty$. Generally, the microgravity (low opposed-flow speeds) data [9,10] fell to the right of the curve in Fig. 5, while the normal-gravity (high opposed-flow speeds) data [20] fell to the left. Estimates of the Blasius boundary-layer thickness ahead of the flames in those experiments suggest that they propagated inside a boundary layer (except the quiescent microgravity case, which has none). Mixed forced- and buoyant-flow flames have been characterized using U_∞ plus an estimate of the boundary-layer structure [22], which depended upon the near-wall velocity gradient. It remains unclear whether the flames of Refs. 9, 10, and 20, particularly the microgravity flames, were deep enough in their boundary layers to be affected only by the near-wall gradient or by more of the velocity profile, since the flame standoff distances were not quantified.

We sought to obtain estimates of acceleration levels where quenching of partial-gravity flames would occur. Mindful of the uncertain comparison of forced and buoyant cases we have described, we used the flammability limits observed in forced flows at microgravity to estimate partial-gravity flammability limits. Figure 6 shows an approximate flammability map for opposed-flow flames, including the data of Fig. 1 plus near-limit microgravity data [9,10], where each is characterized by $V_\infty = V_b$ or U_∞. Adjustments to U_∞ values for boundary-layer influences, even substantial fractional reductions, would not change the position of the flammability curve appreciably. Within the limitations we have discussed, the forced-flow data suggest that quenching of partial-gravity flames should be observable at acceleration levels of $\approx 10^{-3}$–10^{-2} g in 14% oxygen, $\approx 10^{-4}$–10^{-3} g for 15% oxygen, and $\approx 10^{-6}$–10^{-5} g for 21% oxygen.

Conclusions

Using parabolic trajectories in aircraft, we have conducted the first experiments in buoyant diffusion flame spread over a thin solid in a partial-gravity range of 0.05–0.6 times normal earth gravity. Successful operation in this unusual environment required the development of special apparatus and techniques, including a schlieren system for imaging dim near-limit flames, a fast acting and repeatable ignition system, precise acceleration measurements,

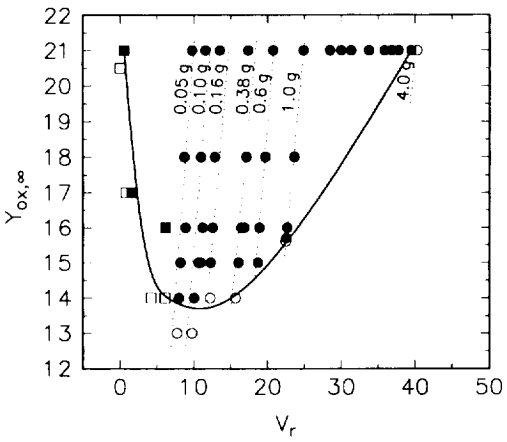

FIG. 6. Estimated flammability map in O_2 mole fraction vs opposed-flow velocity for thin cellulosic fuel. Flow velocities included purely buoyant, V_b, for g/g_{earth} levels shown (circular symbols, >1 g from Ref. 12), and free-stream velocity, U_∞, for microgravity forced-flow tests (square symbols [9,10]). Solid symbols represent flammable conditions; hollow symbols represent nonflammable conditions.

and extending the range of accelerations provided by the aircraft flight crew.

Using gravity as a variable parameter provided a new means to study the effect of convection on flame spread and extinction processes. Unlike experiments in forced flow where the local velocity in front of the flame depends both on the free-stream velocity and the developing boundary layer, the local velocity in front of the flame in buoyant flow depends only on the gravity level.

Downward-spreading flames were observed in partial gravity in O_2/N_2 mixtures between 14% O_2 and 21% O_2 at normal atmospheric pressure, demonstrating peak values of flame-spread rate and increased flammability at local accelerations below normal earth gravity. Flame-spread rates 20% higher than in normal gravity were observed in partial gravity, and flammability increased, with the limiting oxygen fraction falling from 15.6% O_2 in normal gravity to 13–14% O_2 at 0.05–0.1 g.

A data presentation with a radiative correction to dimensionless downward flame-spread rates correlates with Damkohler numbers in purely buoyant flows from 0.05 g to 4.25 g. Comparisons with our data support the qualitative results of theoretical models that include finite-rate chemical kinetics and radiative transport to describe the flame spread and extinction processes. The experimental data provide the basis for improving quantitative predictions from the models.

Acknowledgments

JST would like to gratefully acknowledge the support for his work under NASA Grant No. NAG3-1046. KRS would like to acknowledge the contributions of many associates at the NASA Lewis Research Center, most notably R. Sotos, K. Stambaugh, D. Gotti, D. Griffin, P. Greenberg, and P. Ferkul, and helpful discussions with R. Altenkirch. Finally, both authors would like to acknowledge the support for the work by the Microgravity Science and Applications Division of NASA Headquarters.

REFERENCES

1. Fernandez-Pello, A. C., and Hirano, T., *Combust. Sci. Technol.* 32:1–31 (1983).
2. Di Blasi, C., *Prog. Energy Combust. Sci.* 19:71–104 (1993).
3. T'ien, J. S., *Combust. Flame* 65:1,31–34 (1986).
4. Bhattacharjee, S., and Altenkirch, R. A., Combust. Flame 84:160–169 (1991).
5. Bhattacharjee, S., and Altenkirch, R. A., *Twenty-Third Symposium (International) on Combustion*, The Combustion Institute, Pittsburgh, 1991, p.1627–1633.
6. Chen, C. H., and Cheng, M. C., *Combust. Sci. Technol.* 97:63–83 (1994).
7. Di Blasi, C., Crescitelli, S., Russo, G., and Fernandez-Pello, A. C., *Combust. Sci. Technol.* 64:289–294 (1989).
8. West, J., Bhattacharjee, S., and Altenkirch, R. A., *Combust. Sci. Technol.* 83:233–244 (1992).
9. Olson, S. L., Ferkul, P. V., and T'ien, J. S., *Twenty-Second Symposium (International) on Combustion*, The Combustion Institute, Pittsburgh, 1988, pp. 1213–1222.
10. Olson, S. L., *Combust. Sci. Technol.* 76:233–249 (1991).
11. Bhattacharjee, S., Altenkirch, R. A., and Sacksteder, K. R., *Combust. Sci. Technol.* 91:4–6,225 (1993).
12. Altenkirch, R. A., Eichhorn, R., and Shang, P. C., *Combust. Flame* 37:71 (1980).
13. Weiland, K. J., "Intensified Array Camera Imaging of Solid Surface Combustion Aboard the NASA Learjet," NASA TM-105361, 1992.
14. Grayson, G., Sacksteder, K. R., Ferkul, P. V., and T'ien, J. S., *Microgravity Sci. Technol.* VII:2 (1994).
15. Sarner, Stanley F., *Propellant Chemistry*, Reinhold Pub. Co., New York, 1966, p. 283.
16. Buchele, D. R., and Griffin, D. W., *Appl. Optics* 32:4218–4222 (1993).
17. "JSC Reduced Gravity Program User's Guide," NASA Johnson Space Center Document JSC-22803, 1991.
18. DeLombard, R., Finley, B. D., and Baugher, C. R., "Development of and Flight Results from the Space Acceleration Measurement System (SAMS)," NASA TM-105652, 1992.
19. deRis, J. N., *Twelfth Symposium (International) on*

Combustion, The Combustion Institute, Pittsburgh, 1969, pp. 241–252.

20. Fernandez-Pello, A. C., Ray, S. R., and Glassman, I., *Eighteenth Symposium (International) on Combustion*, The Combustion Institute, Pittsburgh, 1981, pp. 579–589.
21. Frey, A., and Tien, J. S., *Combust. Flame* 36:33 (1976).
22. Altenkirch, R. A., and Vedha-Nayagam, M., *Twenty-Second Symposium (International) on Combustion*, The Combustion Institute, Pittsburgh, 1988, pp. 1495–1500.

COMMENTS

Paul Ronney, University of Southern California, USA. Your radiation parameter does not include a Planck absorption coefficient, which indicates that you are not considering gas-phase radiation. One then infers that your radiation parameter refers to surface radiation with constant emissivity. Do you believe that the quality of your correlation then suggests that surface radiation is more important than gas-phase radiation?

Author's Reply. The radiation parameter, S_R, indicates the increased importance of radiation losses to the environment as the convecting flow velocity decreases. For the low-speed flow conditions observable only in reduced gravity, we have used S_R to compensate the dimensionless flame spread rate for these radiative losses. Without a third parameter to account for radiative loss, dimensionless spread rates in low-speed flows do not correlate well with Damköhler number, despite the success of this approach for higher-speed flows.

The form of S_R used in the correlation seems to suggest that gas-phase radiation loss is not important in the range of conditions tested. This S_R describes loss from the fuel surface and is proportional (for a 2D flame) to $g^{1/3}$. Because gas-phase radiation loss grows with the flame volume, a gas-phase S_R is proportional (for a 2D flame) to $g^{2/3}$. Consequently, while at normal gravity gas-phase loss is much smaller than surface loss, gas-phase loss is amplified with respect to surface loss as gravity becomes small. Numerical modeling (e.g., Ref. 6 in the text) predicts that at sufficiently low gravity, spread rates with gas-phase loss are lower than spread rates with surface loss. We suggest that the lowest partial-gravity level available in the aircraft tests (i.e., 0.05 g_{Earth}) is not low enough for gas-phase loss to dominate spread rate behavior.

●

S. Bhattacharjee, San Diego State University, USA. You evaluated the flame temperature that appears in the deRis/Delichatsios formula using STANJAN, while the original solution requires the use of linearized adiabatic stoichiometric flame temperature. The differences between these two temperatures are quite large, especially at high oxygen concentrations. If the linearized adiabatic temperature was used, how would that affect your correlations?

Author's Reply. In developing the correlation presented in this paper, we first reproduced the correlation of flame spreading presented in Altenkirch et al. [12] in which a calculated stoichiometric, adiabatic flame temperature with no dissociation appeared in the formulation of the Damköhler number, *Da*, and dimensionless spread rate, V_f°, for purely buoyant flows. These temperatures are very high (e.g., 2822 K at 21% oxygen mole fraction) compared with realistic flame temperatures, but serve to represent the release of all conceivably available energy to maintain the flame reactions and drive the buoyant flow.

In that formulation, V_f° approaches unity as *Da* increases, in accordance with the scaling of the measured spread rates with the spread rate at the condition of the maximum conceivable forward heat transfer rate, and the data, over a wide range of atmospheric oxygen content, lie along a smooth curve. Modifying Altenkirch's formulation only by allowing for dissociation in the stoichiometric, adiabatic flame temperature calculation (e.g., 2182 K at 21% oxygen) disrupts the smooth curve seen in Ref. 12, creating a family of curves that differ by oxygen content. However, when the partial-gravity data we obtained are included in this formulation a useful property emerges: blowoff extinctions occur at very similar *Da* for 21% oxygen mole fraction at 4.25 times normal Earth gravity (g), 15.7% oxygen at 1 g, and 15% oxygen at 0.6 g. Introducing the radiation parameter, S_R, removes the oxygen-content dependence of the dimensionless spread rate (incidentally, using $1/V_r$ without the gas properties in S_R does not succeed). The combination of using realistic flame temperatures and correcting the dimensionless spread rate for radiation losses provides a correlation that is independent of gravity level and oxygen content over wide ranges of these dimensional parameters.